THE ASTRONOMICAL JOURNAL VOLUME 111, NUMBER 6 JUNE 1996

A NEAR-INFRARED SPECTRAL IMAGING STUDY OF T TAU

T. M. HERBST, S. V. W. BECKWITH, AND A. GLINDEMANN
Max-Planck Institut für Astronomie, Königstuhl 17, 69117 Heidelberg, Germany
Electronic mail: herbst@mpia-hd.mpg.de

L. E. TACCONI-GARMAN, H. KROKER, AND A. KRABBE
Max-Planck Insititut für Extraterrestrische Physik, Giessenbachstrasse, 85748 Garching, Germany

Received 1996 January 26, revised 1996 February 27

ABSTRACT

We present K (2.01–2.42 μm) and H (1.5–1.8 μm) band imaging spectroscopy of the complex environment of the young stellar object, T Tau. These observations reveal at least five distinct sources of molecular hydrogen emission in the central 4×4 arcsec of the system, including knots of emission centered on the primary and infrared companion, an east-west jet, and what appears to be a Herbig–Haro object located within 3″ of the binary. We detected the latter object in 11 different quadrupole lines of molecular hydrogen, as well as in two H band forbidden transitions of Fe II. The H_2 spectral line ratios point to shock heating with a variety of excitation temperatures. The images also demonstrate that the Brγ emission is point-like and centered on the primary star only. We discuss the nature and origin of the line radiation, the relationship between the outflows and the stars, and the apparent lack of UV fluorescent excited H_2.

1. INTRODUCTION

Observations at infrared wavelengths over the last twenty years have demonstrated the danger in adopting a single astronomical source as a paradigm or representative member of a class of objects. For example, *IRAS* satellite observations of the star α Lyra revealed an unusual disk of large particles orbiting around the star and producing a significant infrared excess on this photometric "standard." Similarly, T Tauri is the prototype of the class of pre-main-sequence objects known as the T Tauri Stars (TTS), yet it is now evident that T Tau is very unusual and perhaps unique.

Beckwith *et al.* (1978) searched five young stellar objects for the 2.12 μm $v=1$–0 $S(1)$ line of molecular hydrogen and discovered it in only one source, T Tau. This star remains one of the few TTS with detectable H_2. One-dimensional speckle interferometry by Dyck *et al.* (1982) revealed an unusual, extremely red companion ~0.6 arcsec south of the visible star. This object is completely obscured for $\lambda \lesssim 1$ μm, yet the so-called T Tauri Infrared Companion (IRC), is brighter than the primary at radio wavelengths and may dominate the overall energetics of the system (Schwartz *et al.* 1984, 1986; Ghez *et al.* 1991; Koresko *et al.* 1996). Despite exhaustive searches, only half a dozen additional Infrared Companion systems have been found. Finally, T Tauri exhibits an unusually complex system of multiple jets and outflows unlike that seen in any other TTS. High resolution, long slit spectra of visible wavelength forbidden lines reveal perhaps half a dozen distinct kinematical structures within the central 10″ of the T Tau binary (Böhm & Solf 1994).

Disentangling these complex phenomena requires both spatial and spectral information. This paper presents new imaging spectroscopy measurements of the T Tauri system taken with the MPE 3D instrument and the CHARM tip-tilt module in the K (2.0–2.4 μm) and H (1.5–1.8 μm) photometric bands. This is not the first infrared imaging spectroscopy study of the T Tauri system. For example, van Langevelde *et al.* (1994) present an image approximately 1 arcmin square of T Tau in the $v=1$–0 $S(1)$ line of molecular hydrogen. Our observations naturally complement their investigation, since they provide complete H and K band spectral coverage. In addition, the central ~5″ of the van Langevelde map are blanked out due to saturation, and the 3D field covers 8×8 arcsec surrounding T Tau.

2. OBSERVATIONS

We observed T Tau on 1995 January 21 in the K band and on 1995 January 11 in the H band. On both occasions, we used the MPE 3D imaging spectrometer and the CHARM tip-tilt module mounted at the $f/10$ Cassegrain focus of the 3.5 m telescope on Calar Alto, Spain.

Weitzel *et al.* (1996) describe the imaging spectrometer in detail. The 3D instrument contains a pair of segmented mirrors which act as a focal plane image slicer, projecting 16 slitlets onto the entrance aperture of a spectrograph. A collimating mirror directs the light to a direct-ruled KRS5 grism, and a camera lens images the resulting spectra onto a 256 ×256 HgCdTe NICMOS3 detector. The output is 256 separate spectra of a 16×16 pixel field. For the Calar Alto observations, each pixel was 0.52 arcsec square and the frames covered the entire K or H band in a single exposure with spectral resolution $R \sim 1000$ ($\lambda/\Delta\lambda$).

Glindemann *et al.* (1996) describe CHARM, the Camera High Angular Resolution Module. This device contains a

 0004-6256/96/111(6)/2403/12/$6.00

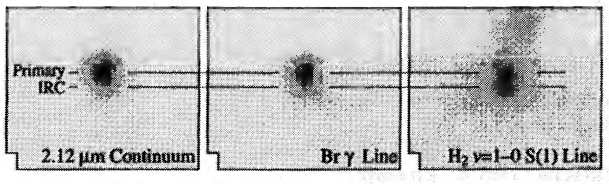

FIG. 1. A slice of the K band data cube centered on 2.12 μm continuum (left), along with continuum-subtracted frames in the $n=7$–4 Brγ line of atomic hydrogen (center), and the $v=1$–0 $S(1)$ transition of H_2 (right). In this and all other figures, the pixels have been resampled to 0.26 arcsec, with north up and east to the left. The guide lines indicate the declinations of the primary star and the infrared companion. The binary is aligned almost exactly north-south, with the IRC displaced slightly to the east. Note that the Brγ distribution follows the continuum, while the $S(1)$ emission is extended.

folded, five-reflection optical train, which forms an image of the telescope entrance pupil on a piezoelectrically driven tip-tilt mirror. One of the folding mirrors is dichroic, allowing visible wavelength radiation to pass through to a CCD-based wave-front sensor. A computer program measures the guide star approximately 30 times per second and drives the tip-tilt mirror to eliminate image motion. For this experiment, T Tau was bright enough at visible wavelengths to serve as its own guide star.

Standard techniques of sky subtraction and flat fielding removed background emission, dark current, and pixel-to-pixel gain variations. We observed several bright standard stars at similar airmass to T Tau, and processed their spectra in an identical manner to produce photometric and spectroscopic references. Division by the spectroscopic standard and subsequent multiplication by a Planck function with the same effective temperature as the reference star eliminated telluric features and produced the correct spectral slope across the band. We used the MPE 3D data reduction utilities to average the individual exposures and to reassemble the resulting spectra in a so-called "data cube." This structure consists of 300 separate wavelength slices, each containing the spatial information over a ~8×8 arsec region.

3. IMAGES

The combination of CHARM and favorable seeing conditions led to excellent images for the K band observations of January 21, approximately 0.″7 full width at half maximum (FWHM). A significant elongation of the stellar image and southward shift of the centroid indicate that we are beginning to see the infrared companion at the longest wavelengths, despite the relatively large pixels (0.″52) compared to the binary separation (0.″69, Ghez *et al.* 1995).

Fitting the spectral baseline on a pixel-by-pixel basis allows us to generate continuum-subtracted images centered at the wavelengths of important spectral lines. Figure 1 shows the 2.12 μm continuum along with two such images in the $n=7$–4 (Brγ) recombination line of atomic hydrogen, and in the $v=1-0S(1)$ quadrupole line of H_2. The Brγ emission is spatially unresolved and appears centered on the visible component of the binary, T Tau N. The molecular hydrogen, on the other hand, is more diffuse, and a distinct knot of emission appears to the northwest of T Tau. Unlike the atomic gas, a significant fraction of the H_2 emission in T Tau comes from the vicinity of the southern object, the infrared companion.

A logarithmic stretch of the $S(1)$ line image reveals the spatial distribution of the fainter molecular hydrogen emission near T Tau. Figure 2 (Plate 141) superimposes the 2.12 μm continuum (contours) on the faint H_2 (false color). In this presentation, a filamentary structure extends from T Tau to the west, with a shorter, complementary filament appearing to the east. Not so clearly visible in this image is a diffuse H_2 component, which essentially fills the frame.

We detected the T Tau system, and particularly the NW knot, in a number of additional K band transitions of molecular hydrogen. The availability of both spectral and spatial information is critical in detecting and identifying these features, particularly in the northwest knot and for those lines which are faint or which occur at wavelengths of reduced atmospheric transparency.

A combination of poor seeing and shorter integration time reduced our sensitivity for the H band measurements of January 11. Nevertheless, we unambiguously detected the 1.75 μm $v=1-0S(7)$ H_2 line throughout the frame, and saw the 1.644 μm Fe II line in the NW knot. Figure 3 (Plate 141) shows the continuum-subtracted Fe II frame in false colors with the $v=1-0S(1)$ contours from Fig. 2. Note that the peak of Fe II emission lies closer to the central stars than does the H_2.

4. SPECTRA

Viewing the data cube signal in a direction perpendicular to the image planes produces conventional spectra. The traces in Fig. 4 represent the total flux in a 2.″3 square box centered on the stars, in a 2.″9×1.″8 aperture containing the NW knot, in a synthetic aperture isolating the west filament, and in all regions devoid of emission from the other components. The vertical bars and labels indicate the locations of clearly detected spectral lines. The relative lack of such features in the stars is due in part to the bright continuum and the inability to confirm a detection on the basis of morphology, i.e., a spatially coherent structure at the correct location and which is absent at adjacent wavelengths.

Table 1 lists the line fluxes and uncertainties based on nonlinear, least-squares fits of Gaussian profiles to the spectra of Fig. 4. Figure 5 shows some representative Gaussian fits. The model includes five parameters: the central wavelength λ_0, the amplitude A, the σ of the Gaussian, and two parameters, m and b giving the slope and intercept of the linear baseline, respectively. With the model $F_\lambda = b + m\lambda + A\exp[-(\lambda-\lambda_0)^2/2\sigma^2]$, the flux is given by $\sqrt{2\pi}A\sigma$ and the formal uncertainty is $\Delta F = [2\pi(\sigma^2\Delta A^2 + A^2\Delta\sigma^2)]^{1/2}$, where ΔA and $\Delta\sigma$ are those changes in the A and σ parameters which increase the χ^2 per degree of freedom by 1 (Bevington 1969). The calculations assumed error bars on the original measurements of ~1%, based on the point-to-point variations of the signal in nearby regions of the spectrum known to be free of lines. This choice is supported by the quality of the fits (Fig. 5), and the fact that the reduced χ^2 was always near 1. Although

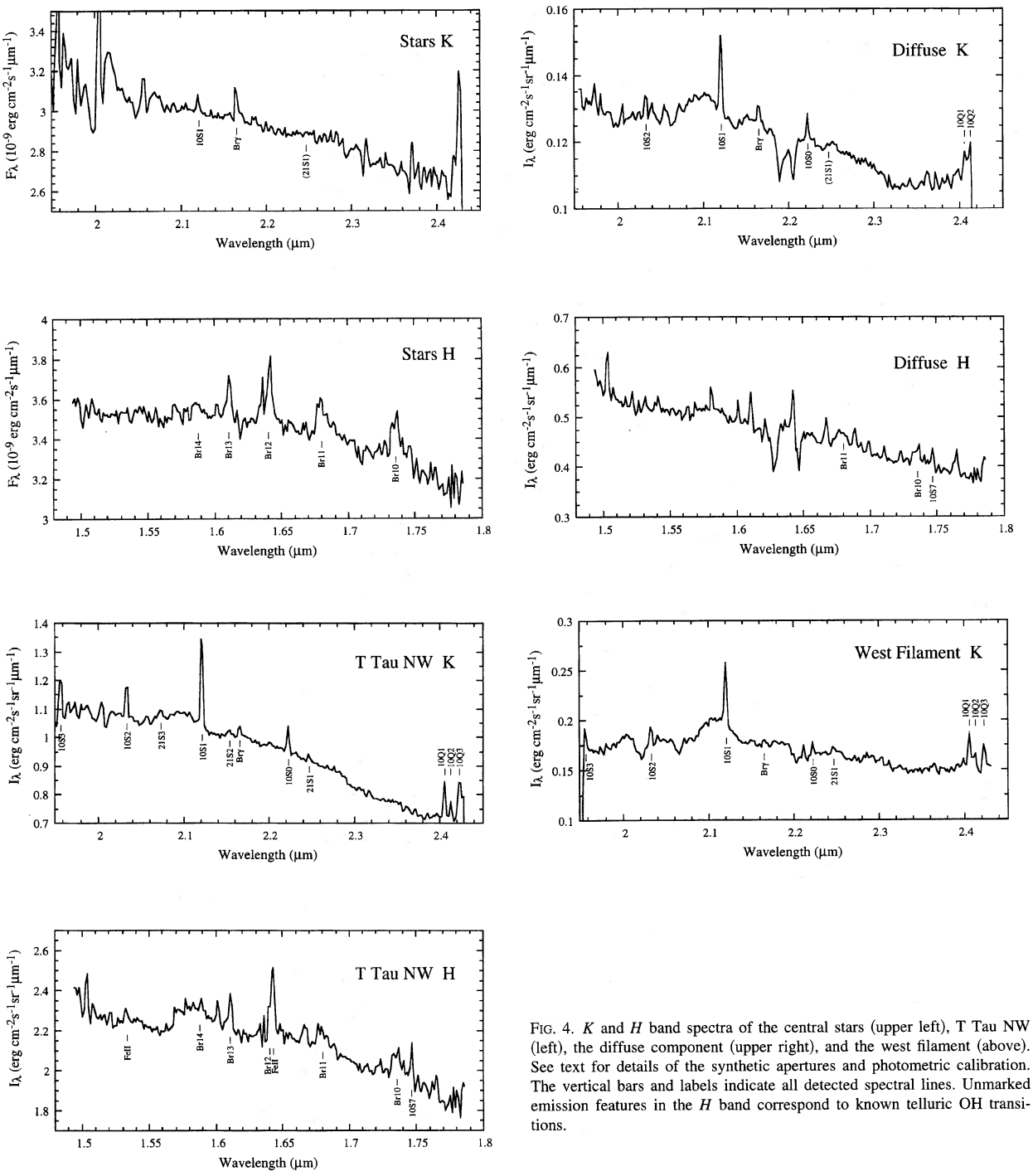

FIG. 4. *K* and *H* band spectra of the central stars (upper left), T Tau NW (left), the diffuse component (upper right), and the west filament (above). See text for details of the synthetic apertures and photometric calibration. The vertical bars and labels indicate all detected spectral lines. Unmarked emission features in the *H* band correspond to known telluric OH transitions.

the brightness of the photometric standard is also known to better than 1% (Bouchet *et al.* 1991), a number of additional effects increase the estimated absolute uncertainty of the K band line measurements to $\lesssim$5%. These effects include the lack of an airmass correction, and differences between the *K* magnitudes synthesized from a spectrum and the "true" filter values. Note that the uncertainties in Table 1 do not include these systematic effects.

Most of the flux fits listed in Table 1 come from the original ratioed spectra (i.e., T Tau/spectroscopic standard). Several H_2 lines lie in regions of very poor atmospheric transmission, however, and in these instances, small differences between the airmass of T Tau and the reference star produce large artifacts in the resulting ratio. For these transitions, we added a constant offset to the spectroscopic standard spectrum to give the same equivalent width of telluric absorption as in T Tau. Treating the photometric standard in the same manner produces accurate line fluxes, a result we

TABLE 1. Derived H and K band line fluxes for the components of T. Tau.

Line	Wavelength (μm)	Stars (10^{-13} erg cm^{-2} s^{-1})	T Tau NW (10^{-4} erg cm^{-2} s^{-1} sr^{-1})	West Jet (10^{-4} erg cm^{-2} s^{-1} sr^{-1})	Diffuse (10^{-4} erg cm^{-2} s^{-1} sr^{-1})
Fe II	1.53390	...	2.06 ±0.26	...	...
Br 13	1.61093	6.9 ±1.4	...	...	...
Br 12	1.64072	11.7 ±1.6	...	...	...
Fe II	1.64355	...	10.8±1.6	...	...
Br 11	1.68065	13.8 ±1.2	5.2±1.1	...	...
Br 10	1.73621	7.0 ±1.3	4.0±1.0	...	...
1–0 $S(7)$	1.74750	3.45±0.53	3.44±0.84	...	0.69±0.20
1–0 $S(3)$*	1.95702	...	6.7±1.7	...	...
1–0 $S(2)$*	2.03320	...	4.26±0.46	0.71±0.11	0.22±0.11
2–1 $S(3)$*	2.07290	...	1.81±0.85	...	...
1–0 $S(1)$	2.12125	3.30±0.30	12.3±0.4	2.56±0.10	0.890±0.033
2–1 $S(2)$	2.15360	...	0.58±0.12	...	...
Brγ	2.16550	12.7 ±0.7	1.101±0.089	0.133±0.015	0.179±0.004
1–0 $S(0)$	2.22268	...	3.02±0.18	0.482±0.093	0.245±0.013
2–1 $S(1)$	2.24710	...	0.737±0.087	0.212±0.025	...
1–0 $Q(1)$*	2.40593	...	4.40±0.34	0.93±0.41	0.15±0.14
1–0 $Q(2)$*	2.41278	...	1.83±0.97	0.32±0.13	...
1–0 $Q(3)$*	2.42307	...	9.9±1.8	0.99±0.28	...

*Located in a region of poor atmospheric transparency. Formal uncertainty tripled.

verified by comparing the derived fluxes for those H_2 lines which are free of telluric absorption. As an added precaution, we tripled the calculated uncertainties in Table 1 for all potentially contaminated lines.

The ratios of molecular hydrogen transitions arising from the same upper level can in principle give the line of sight extinction A_V to the emitting region (e.g., Beckwith *et al.* 1979; Scoville 1982). For example, the $v=1-0S(1)$ and the $v=1-0Q(3)$ lines share the same upper level ($v=1$, $J=3$). The ratio $S(1)/Q(3)$ then depends on the Einstein A coeffi-

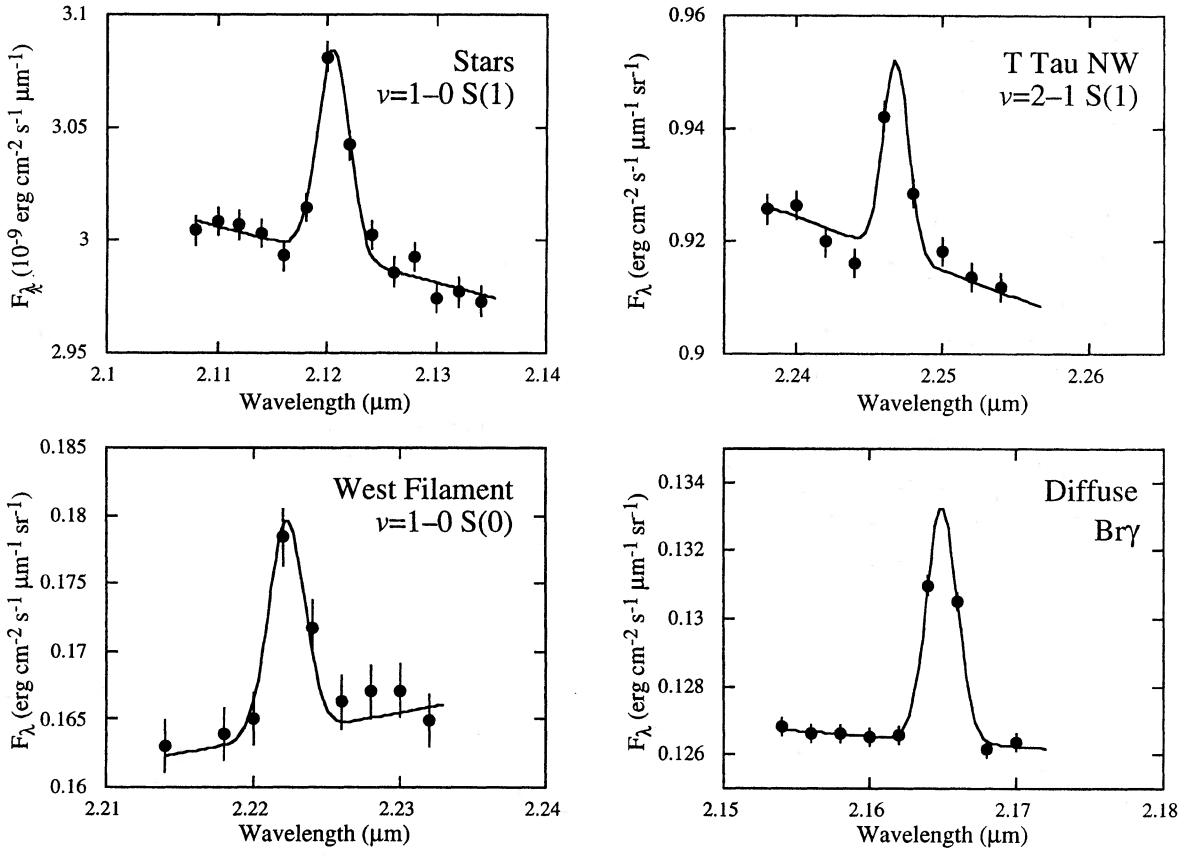

FIG. 5. Representative line fits. See text for fitting procedure and Table 1 for derived fluxes.

cients and the extinction, and is independent of temperature. For a single, optically thin, transition at wavelength λ, the line intensity I is given by

$$I=\frac{Ahc}{4\pi\lambda}N_u 10^{-0.4A_\lambda}, \quad (1)$$

where A is the Einstein A coefficient, N_u is the number of molecules in the upper state, and A_λ is the extinction. The ratio of two lines with the same upper level gives the selective extinction E between the wavelengths of the two transitions. Comparison with standard interstellar extinction laws then gives the A_V to the gas. For the $v=1-0S(1)$ and $Q(3)$ lines, $E=2.5\log(1.426\cdot I_{Q3}/I_{S1})$, where the subscripts refer to the appropriate spectral line, and we have adopted the Einstein coefficients from Turner *et al.* (1977). Using $A_\lambda/A_V\sim\lambda^{-1.64}$ and $A_K/A_V=0.112$ (Rieke & Lebofsky 1985), the visual extinction is:

$$A_V=108\log\left(1.426\cdot\frac{I_{Q3}}{I_{S1}}\right).$$

For the NW knot fluxes in Table 1, $A_V=1.1$, somewhat lower than previous determinations toward the photosphere of T Tau itself ($A_V\sim1.4$, Cohen & Kuhi 1979; Adams *et al.* 1988). Poor atmospheric transmission at the wavelength of the $Q(3)$ line is the major source of uncertainty in this determination. In the following, we adopt $A_\lambda\propto\lambda^{-1.64}$ and $A_{S1}=0.16$.

5. COMPONENTS OF THE T TAU SYSTEM

At least five distinct components appear in the molecular hydrogen channels: the northwest knot, the two stars themselves, the west filament, and the diffuse emission. The following paragraphs discuss each of these components in detail.

5.1 T Tau NW

The most obvious structure in the data cubes after T Tau itself is a bright knot of line emission approximately 2″ to the northwest of the binary. This feature, which we call T Tau NW, is likely related to the extended H_2 emission seen in Fig. 1 of van Langevelde *et al.* (1994), although much of the knot lies within the blanked-out region at the center of their map. T Tau NW accounts for approximately one third of the total $v=1-0S(1)$ line flux in the central few arcseconds, confirming the importance of extended emission (Beckwith *et al.* 1978).

The lack of bright continuum and the ability to correlate spatial and spectral information increased our sensitivity to faint features at the location of the northwest knot, and we detected a total of 11 K and H band molecular hydrogen lines in addition to Brγ and the $a^4D_{7/2}-a^4F_{9/2}$ transition of Fe II at 1.644 μm. The simultaneous spatial and spectral information allows an unambiguous identification of coherent structure, and thereby distinguishes between line emission arising from T Tau NW and that from the underlying diffuse component. Occasionally, the spatial distribution varies from line to line, giving hints to the underlying physical mechanisms powering and shaping the source. The following sections discuss each of the molecular and atomic species detected in T Tau NW:

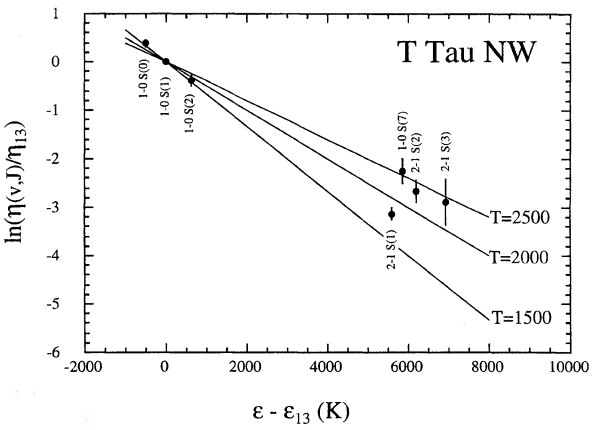

FIG. 6. Column density per degenerate sublevel versus energy difference for T Tau NW. This plot shows those transitions free of atmospheric absorption relative to the $v=1-0$ $S(1)$ line (the "13" subscript refers to the $v=1$, $J=3$ upper level). In LTE, the points should fall on a straight line with slope inversely proportional to excitation temperature as shown. The $v=1-0$ transitions give $T_{exc}\lesssim2000$ K, while the $v=2-1$ lines point to a higher excitation temperature.

5.1.1 Molecular hydrogen—1.95–2.42 μm

Quadrupole emission lines from H_2 dominate the K band spectrum of T Tau NW. Molecular hydrogen emission arises in a number of physical processes, the most common of which are shock excitation and ultraviolet fluorescence (see Shull & Beckwith 1982, and references therein). The ratio of the $v=1-0S(1)$ line to the $v=2-1S(1)$ line can discriminate between these two mechanisms. Shock calculations predict a ratio of 5:1 or more, while ultraviolet fluorescence models give a ratio closer to 2:1. The 1–0/2–1 $S(1)$ ratio is $\gtrsim15$ for T Tau NW, arguing strongly that the molecular hydrogen is heated in shocks. Further discussion of the role and diagnostics of ultraviolet fluorescence appears in Sec. 9.

The extinction-corrected line strengths in Table 1 can give the excitation temperature under the assumption of local thermodynamic equilibrium. In these conditions, the column density per degenerate sublevel $\eta_{v,J}$ is

$$\eta_{v,J}\equiv\frac{N(v,J)}{g_{v,J}}=\frac{N_{\rm tot}}{Z(T)}\cdot e^{-\epsilon_{v,J}/T}, \quad (2)$$

where $N(v,J)$ and $N_{\rm tot}$ are the sublevel and total column densities, respectively, $g_{v,J}$ is the degeneracy, ϵ is the upper state energy expressed in K,T is the excitation temperature, and Z is the partition function. Forming the ratio of $\eta_{v,J}$ to that of a reference transition, (i.e., η_{S1}), eliminates several of these quantities, giving $\ln(\eta_{v,J}/\eta_{S1})=-1/T\cdot(\epsilon_{v,J}-\epsilon_{S1})$.

We proceed on the assumption (discussed below) that the ortho-to-para hydrogen ratio is 3:1, which is characteristic of H_2 formed at $T>100$ K (McQuarrie 1976). In this instance, the degeneracy g is $(2J+1)$ for even J states (para-hydrogen) and $3(2J+1)$ for odd J states (ortho-hydrogen). Figure 6 plots $\ln(\eta_{v,J}/\eta_{S1})$ against the energy level differ-

ence for the H_2 lines in the NW knot. A single linear fit with excitation temperature ~2000 K models the emission lines well, although there is some evidence of a flattening for the $v=2-1$ transitions; fitting the $v=1-0$ lines alone gives $T\sim1500$ K. This suggests a range of rotational temperatures, with the lower excitation 1–0 lines tracing the cooler regions and the 2–1 transitions produced in hotter gas. There is no significant difference in the spatial distribution of these two sets of lines, indicating that if the gas exists at multiple temperatures, it is distributed along the line of sight or is well mixed on $\lesssim$0.5 arcsec scales.

We can use this derived temperature to calculate the partition function $Z(T)$ of the molecular hydrogen, and hence the total column density $N_{\rm tot}$ of gas via Eqs. (1) and (2). The analytic expression $Z(T)=0.0247T\cdot[1-\exp(-6000/T)]^{-1}$ is an excellent approximation to the true partition function evaluated by summing all transitions with $\epsilon\lesssim25\,000$ K. The column density of molecular hydrogen based on the intensity I_{S1} of the $v=1-0S(1)$ line is then

$$N_{\rm tot}=4.55\times10^{16}T\cdot(e^{6000/T}-1)e^{956/T}\cdot I\cdot10^{0.4A_\lambda}. \quad (3)$$

$N_{\rm tot}$ is 3.0×10^{18} cm^{-2} for $T=2000$ K, $I_{S1}=1.23\times10^{-3}$ erg cm^{-2} s^{-1} sr^{-1}, and $A_{S1}=0.16$. With a measured size of 1.″6×2.″1, T Tau NW is spatially resolved in Fig. 2. These dimensions and the calculated $N_{\rm tot}$ imply approximately $1.1\times10^{-7}\,\mathcal{M}_\odot$ of molecular hydrogen at the 140 pc distance to the Taurus molecular cloud.

The foregoing calculations assumed an ortho-to-para hydrogen ratio of 3 in order to determine the excitation temperature. Here, we adopt a different approach, assuming a *single* excitation temperature in order to derive the ortho-para ratio. Varying this ratio in the direction of its low-temperature limit (pure para-hydrogen) has the effect of lowering the even-J data points relative to the odd-J transitions in Fig. 6. The goal is then to find the ortho-para ratio which gives a single excitation temperature, i,e., that ratio which produces the best straight line on the plot.

The ortho-to-para ratio is indistinguishable from 3.0 for the $v=1-0$ transitions free of atmospheric absorption. The line fluxes of the 2–1 lines are more uncertain. An ortho to para ratio of 1.5 produces a straight line through the 2–1 points, but this ratio forces the higher signal-to-noise ratio 1–0 transitions out of alignment, and implies an unreasonably high excitation temperature of $\gtrsim$30 000 K.

5.1.2 Atomic hydrogen Brγ—2.166 μm

The K band spectrum of T Tau NW in Fig. 4 also shows an emission feature due to the $n=7-4$ (Brγ) recombination line of atomic hydrogen. This feature is approximately ten times fainter than the $v=1-0S(1)$ line in the 2.″9×1.″8 aperture.

The Brγ transition usually traces excitation conditions that are considerably warmer than the 2000 K derived from the molecular lines in the previous section. A careful examination of the data cube slices centered on the Brγ line reveals *no coherent spatial structure* at the location of T Tau NW, however. The Brγ line in both T Tau NW and the stars displays a slight blue absorption, suggesting that the diffuse emission near T Tau NW arises from scattering of stellar line photons by dust.

5.2 Fe II—1.644 μm

The $a^4D_{7/2}-a^4F_{9/2}$ forbidden line of Fe II at 1.644 μm is a diagnostic of fast, dissociative shocks such as those seen in Herbig–Haro objects (Stapelfeldt *et al.* 1991). Its presence in T Tau NW at a strength roughly half that of the $v=1-0S(1)$ molecular hydrogen line indicates a range of excitation conditions, since a shock which produces Fe II efficiently will destroy the H_2. Several mechanisms can "soften" a shock front for the molecular hydrogen, including magnetic precursors and the geometry of the wind/ambient-material interface.

Images and spectra derived from the H band data cube also show emission from T Tau NW in the 1.534 μm [Fe II] $a^4{}_{5/2}-a^4F_{9/2}$ transition. The ratio of the 1.53–1.64 μm lines provides a temperature-independent diagnostic of electron density. The measured line strengths and the rate coefficients of Pradhan & Zhang (1993) imply $n_e\sim10^4$, although this measurement should be repeated with higher signal-to-noise ratio and under better seeing conditions.

5.3 The Stars

The K band spectrum of the stars in Fig. 4 shows emission lines from both atomic and molecular hydrogen. The $n=7-4$ recombination line at 2.165 μm is a common transition in young stellar objects, tracing regions of high excitation usually identified as ionized wind. Molecular hydrogen features are rarely seen in stars, however. Following the detection of the 2.12 μm $v=1-0S(1)$ line (Beckwith *et al.* 1978), Brown *et al.* (1981, 1984) discovered several ultraviolet transitions of molecular hydrogen in *IUE* spectra centered on T Tau and on Burnham's Nebula to the south. As with the northwest knot, possible H_2 excitation mechanisms include ultraviolet fluorescence and outflow shocks induced when a massive wind from the star encounters the surrounding neutral medium. In addition, infall accompanied by accretion shocks may explain the H_2 emission and unusual spectral properties of some infrared companions (Herbst *et al.* 1995).

5.3.1 Spatial distribution

In contrast to the atomic hydrogen Brγ line, which is spatially unresolved and centered on the primary, the H_2 $v=1-0S(1)$ transition is extended at the location of the two stars. The upper left panel of Fig. 7 shows the region near T Tau in the $S(1)$ line. The emission clearly comes from two distinct knots aligned approximately north-south. A comparison with the short wavelength continuum, which presumably shows the primary star only, and with the known offset to the IRC, demonstrates that these knots correspond well to the locations of the primary and infrared companion.

We applied the Gaussian fitting routine described in Sec. 4 to characterize the spatial distribution of the $S(1)$ line. Fits to one-dimensional cuts give the location and extent of the H_2 knots. Similar tests on the continuum frames indicate that

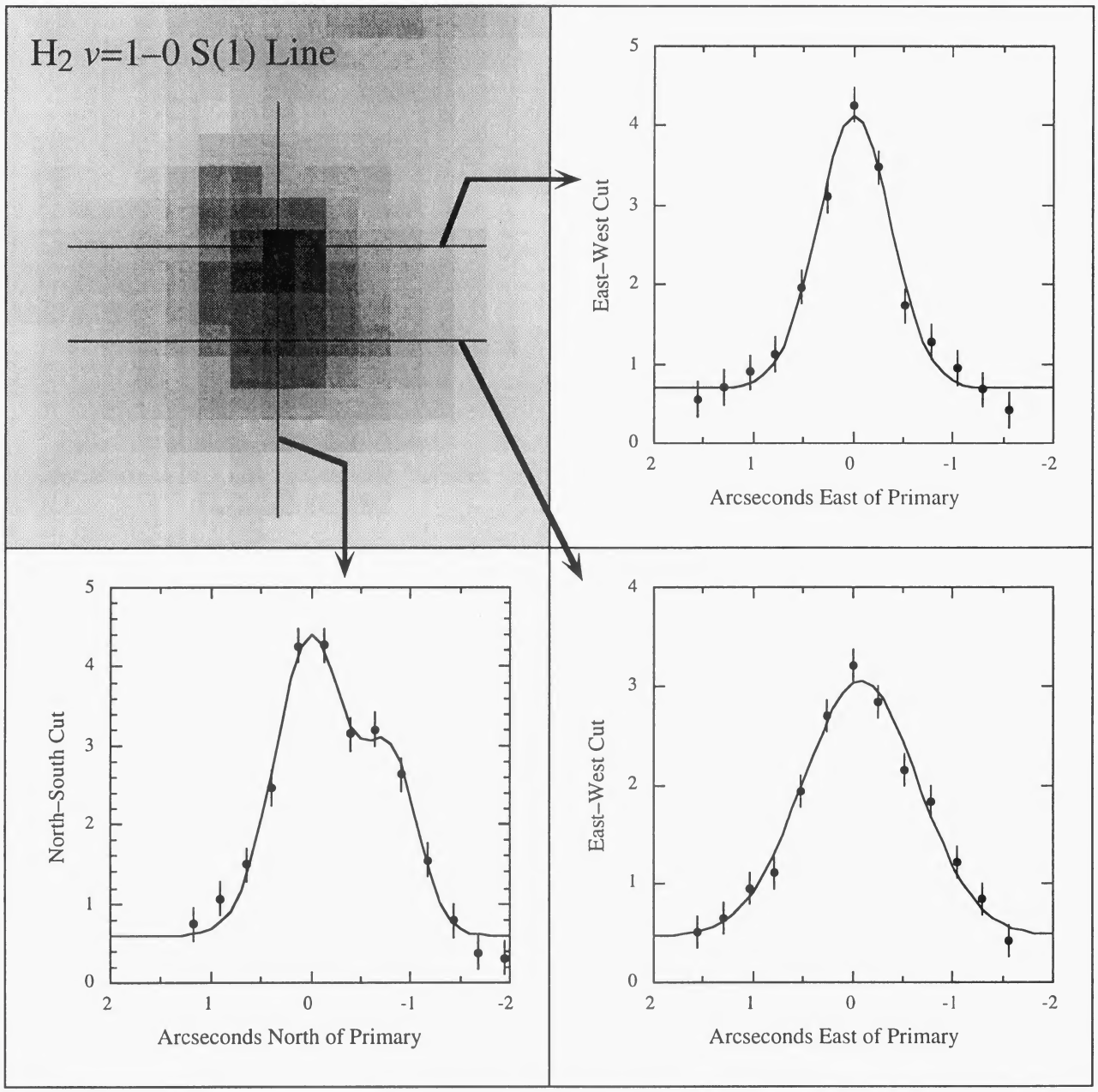

FIG. 7. One-dimensional cuts through the $v=1-0$ $S(1)$ line distribution near the stars. The primary star is spatially unresolved (upper left plot), while the infrared companion is extended east-west (lower right). The $S(1)$ emission associated with the IRC peaks somewhat to the west of the primary, while the companion itself lies slightly to the east. A north-south cut (lower left) shows two spatially unresolved peaks at the locations of the primary and IRC.

the molecular hydrogen emission is coincident with the star and spatially unresolved in T Tau N. On the other hand, the $S(1)$ emission appears extended E-W in T Tau S and is displaced slightly to the west from the known position of the star. This displacement is apparent in the $S(1)$ line image in Fig. 7; the infrared companion lies to the east of the primary, while the H_2 emission peaks somewhat to the west.

Table 1 lists the measured fluxes for the atomic and molecular lines detected in a synthetic aperture enclosing both the primary and the IRC. The complex morphology of the molecular hydrogen $v=1-0S(1)$ emission makes it difficult to divide the flux into separate contributions from T Tau N and T Tau S. Modeling the total line emission as the sum of two Gaussian point spread functions, with the properties shown in Fig. 7, suggests that approximately 50% of the H_2 flux comes from each star.

5.3.2 Excitation mechanism, temperature, and mass

The presence of atomic hydrogen recombination radiation indicates that a large flux of ultraviolet photons may exist in the near environment of T Tau, and thus fluorescence may be an important excitation mechanism for the H_2. As with the northwest knot, the ratio of the $v=1-0S(1)$ to the $v=2-1S(1)$ line can discriminate between the shock heating and UV fluorescence scenarios. Unfortunately, photon noise

from the bright stellar continuum limits our sensitivity for the fainter molecular hydrogen features, including the $v=2-1S(1)$ line. Based on the point-to-point variations in the spectrum near 2.248 μm, the 2–1 line is at least five times fainter (3σ) than the $1-0S(1)$ transition, arguing that this component of the molecular hydrogen is heated in shocks.

The $v=1-0S(1)$ line strength and the upper limit to the 2–1 transition allow an estimate of the maximum excitation temperature of the molecular gas centered on the stars. Placing the appropriate points on Fig. 6 gives $T<2900$ K. The measured $1-0S(1)$ line strength and Eq. (3) imply $N_{\rm tot}\sim 2.8\times10^{18}$ cm^{-2} for $T=2900$ K, rising to $\sim 6\times10^{18}$ cm^{-2} at 2000 K. The total masses of molecular hydrogen centered on the stars in these cases are approximately 1 and 2.5×10^{-7} $\mathcal{M}_\odot$, respectively.

5.4 The West Filament

The final spatially distinct structure in the $v=1-0S(1)$ map is a filament of emission extending to the west from the two stars. This object appears at lower signal to noise in the other bright H_2 transitions as well, but it produces no detectable Brγ emission. The west filament may be associated with a high negative velocity jet detected to the west of T Tau in visible wavelength, longslit spectra of Bührke *et al.* (1986) and Böhm & Solf (1994). Their observations indicated that this jet terminates in and powers the Herbig–Haro object in NGC 1555, approximately 30″ to the west.

The presence of multiple lines of H_2 allows an assessment of the excitation mechanism as before. The $v=1-0/v=2-1S(1)$ line ratio is 12, again arguing for heating in shocks. A plot of $\ln(\eta)$ vs ϵ should give the temperature as in Fig. 6, but the $v=1-0$ line strengths do not lead to a single temperature. The $S(1)$ point lies above the line connecting the $S(0)$ and $S(2)$ measurements (see Fig. 8). As explained in Sec. *5.1.1*, a systematic difference in the column density of even versus odd-J transitions can indicate an ortho-to-para hydrogen ratio different from 3.0. This cannot explain the behaviour in Fig. 8, however, since the required ratio is approximately 4, which is physically impossible. A range in excitation temperatures is also an unlikely cause, since the $v=1-0$ lines have similar upper state energy, and the steepening of the plot with increasing ϵ would indicate that the lower excitation lines arise in a higher-temperature environment.

Partial absorption of the $v=1-0S(2)$ line by the earth's atmosphere can produce the effect seen in Fig. 8. The $S(2)$ transition occurs at 2.0337575 μm (in vacuum, Bragg *et al.* 1982) in a region of the atmosphere filled with absorption features spaced approximately 40 km s^{-1} apart (Livingston & Wallace 1991). A deeper, broader absorption appears at 2.0331 μm, approximately 120 km s^{-1} blueward of the apparent velocity of T Tau as seen from earth on 1995 January 21 (Herbig 1977). We calculated the fraction of flux lost as a function of the intrinsic linewidth and the velocity shift at the source. Telluric absorption can remove as much as 30%–40% of the incident $v=1-0S(2)$ flux for relatively narrow lines (10–20 km s^{-1} FWHM) which are blueshifted by $\sim$120 km s^{-1} relative to T Tau. Lines close to the systemic velocity are affected by 10% or less.

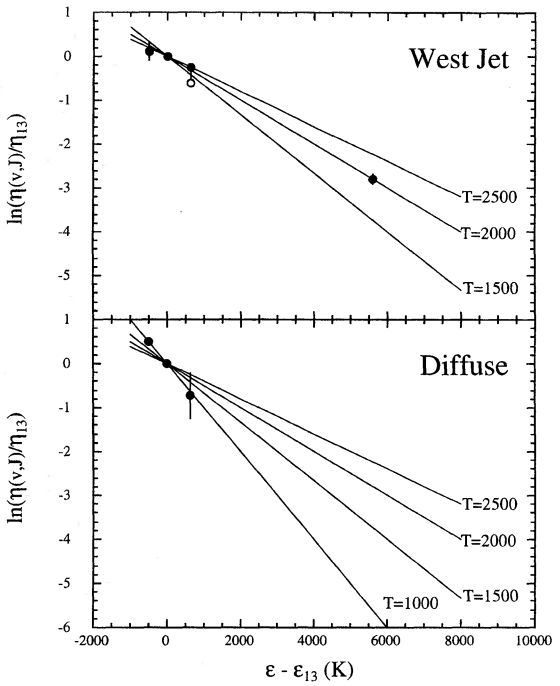

FIG. 8. Same as Fig. 7 for the west filament (top) and the diffuse component (bottom). Possible telluric absorption from blueshifted H_2 can account for the low $v=1-0$ $S(2)$ point for the west filament (open circle). Compensating for this effect moves the open circle upward to the position of the filled circle. See text for details.

Increasing the $S(2)$ flux by 1/0.7 shifts the point as shown in Fig. 8, producing a better linear fit with $T\sim2000$ K. The 3D instrument has insufficient spectral resolution to unambiguously determine the line shift and FWHM of the $S(2)$ line in the west filament, and thus the telluric absorption explanation is tentative. We note, however, that the $v=1-0S(1)$ transition appears with equal strength in two adjacent slices of the data cube everywhere else in the T Tau environment. At the location of the west filament, however, the blueshifted channel dominates. In addition, both Bührke *et al.* (1986) and Böhm & Solf (1994) saw forbidden line emission in this region at a blueshifted velocity of 120 km s^{-1} relative to T Tau.

At a temperature of 2000 K, the $v=1-0S(1)$ flux and Eq. (3) give a total column density of molecular hydrogen in the west filament $N_{\rm tot}\sim6\times10^{17}$ cm^{-2}. This corresponds to approximately 1×10^{-8} $\mathcal{M}_\odot$

5.5 The Diffuse Component

Diffuse continuum and line emission permeates the entire frame in Fig. 2. We isolated the spectrum of this component by multiplying the data cube with a mask containing zeroes at all pixel locations associated with the stars, T Tau NW, and the west filament. The spectra in Fig. 4 represent the flux in the remaining $\sim$50% of the pixels. The diffuse emission around T Tau includes the $v=1-0S(0)$, $S(1)$, and $S(2)$ lines of molecular hydrogen, in addition to Brγ.

Figure 8 plots $\ln(\eta)$ vs ϵ for the three H_2 transitions. The $v=1-0$ lines apparently arise in a relatively cool environ-

ment, with $T \sim 1000$ K. This low temperature and the measured $S(1)$ flux suggest that the diffuse component contains a substantial amount of mass in molecular hydrogen: $N_{tot} = 5 \times 10^{18}$ cm^{-2}, corresponding to $\sim 10^{-6}$ $\mathcal{M}_\odot$.

The qualitatively different $v = 1-0$ line ratios compared to the other components of the T Tau system indicate that the diffuse emission lines occur in the ambient environment and are not scattered from the central sources, (scattering would increase the prominence of shorter wavelength lines, producing a seemingly higher T_{exc}). In addition, the Brγ transition does not display a blue absorption as it does elsewhere in the T Tauri system. The presence of the Brγ recombination line and the H_2 transitions argue that a mixture of molecular and atomic gas coexist along the line of sight.

6. THE NATURE OF T TAU NW AND THE WEST FILAMENT

T Tau NW and the west filament are spatially coherent line emission structures located within 2″ of the binary star T Tau. Their spectral characteristics are quite different from the stars. In particular, they exhibit a much larger line to continuum ratio in the H_2 transitions and a lower T_{exc}. This argues against their being due to light scattered from local enhancements of dust.

The molecular hydrogen line ratios and the presence of Fe II emission suggests that T Tau NW and the west filament are shock excited, and we postulate that these components are the signatures of outflows from the binary star system. Herbig–Haro objects emit both Fe II lines and molecular hydrogen, the latter displaying a range of excitation temperatures (Stapelfeldt *et al.* 1991). The H_2 may arise in shocks within the flow itself, or be heated as the gas strikes the ambient molecular cloud.

The presence of apparent "counter jets" to the SW and E of T Tau support this hypothesis. The counterpart of T Tau NW lies at the lower left edge of Fig. 2, and is quite visible in the larger scale $v = 1-0S(1)$ map of van Langevelde *et al.* (1994). A small protrusion to the ENE of the stars in Fig. 2 may be the counter jet of the west filament. Interestingly, there are significant gaps between the stars and the beginnings of the NW-SE flow system, whereas the E-W system shows no such gaps.

The displacement of the knot of Fe II emission relative to the molecular hydrogen may provide a clue to the excitation of T Tau NW and this mixing of dissociative and nondissociative shocks. Light curve studies of the visually bright star (Herbst *et al.* 1986) suggest that we see T Tau at an inclination angle of 8–13°, i.e., almost pole-on. An outflow or jet emerging from the star along the rotation axis will strike the ambient molecular material and generate a shock front close to the line of site to T Tau. Figure 9 shows a schematic of the shock geometry. The direct impact can dissociate the material and produce the diagnostic Fe II emission at the "working surface," while the oblique wind toward the edge of the flow will produce lower-energy molecular shocks. We should see the Fe II at apex of the shock, and, displaced somewhat further from the star, the edge-brightened molecular hydrogen, (see Fig. 3 and the calculations of Smith 1991).

Kinematic evidence for a complex system of outflows appears in the long-slit spectra of Böhm & Solf (1994). These authors identified at least five distinct velocity structures in long-slit spectra centered on the forbidden [O I], [N II], and [S II] lines near 6500 Å. The spatial location and orientation of these structures suggest that T Tau NW and its counterpart are associated with outflows C and D, while the west filament corresponds to condensation B (see their Fig. 5). Böhm and Solf argue that outflow B shows a higher degree of collimation close to the stars than do C and D, a notion supported by the H_2 morphology of these components. Finally, Böhm and Solf found peaks of [S II] emission approximately 1″ to the NW and SE of T Tau, at locations corresponding to the inside edges of T Tau NW and its counterpart. This high excitation shock line should appear nearer to the stars than the H_2, as does the 1.644 μm Fe II transition.

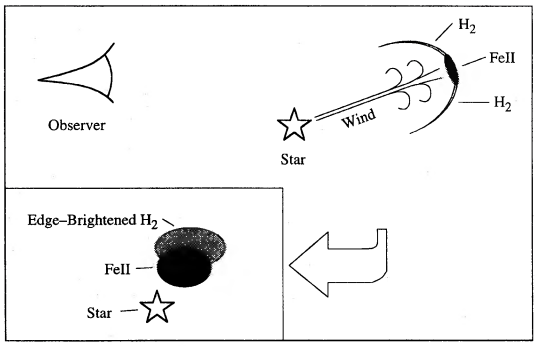

FIG. 9. Cartoon showing possible Herbig–Haro geometry for T Tau NW. A combination of high inclination to the line of sight and a longer pathlength through the upper part of the bow shock produces the observed displacement between the molecular hydrogen emission and the forbidden Fe II at the working surface of the flow.

In summary, T Tau NW appears to be a Herbig–Haro object, based on both spectral and morphological evidence. If T Tau NW is indeed a bow shock inclined ~15° to the line of sight, it lies approximately 1200 AU away from T Tau itself. The positive [S II] velocities in this region and the negative velocities near the SE counterpart suggest that T Tau NW is the more distant, receding part of the flow (Fig. 9). The west filament is also likely an outflow with a counterflow to the ENE, in which case the high negative [S II] velocities to the west of T Tau indicate that the west filament is the nearer, approaching arm. Despite its apparent curvature in Fig. 2, we agree with Bührke *et al.* (1986) and Böhm & Solf (1994) that the west filament eventually powers the Herbig–Haro object in NGC 1555. Partial obscuration of the receding counterpart, which may also be curved, can explain the relative prominence of the two arms of the flow and the complete absence of [S II] emission to the ENE.

7. THE RELATION BETWEEN THE OUTFLOWS AND THE STARS

It is difficult to understand how a single star or star/disk system can produce the two nearly-orthogonal jets associated with T Tau NW and the west filament. This suggests that each star in T Tau powers one outflow, but which star is responsible for which?

Böhm & Solf (1994) attribute the B condensation to the primary on the basis of multiple position angle, long-slit spectroscopy. The infrared companion must therefore produce the C-D outflow. However, this pairing is not so obvious in Fig. 2, if T Tau NW and its SE counterpart correspond to C-D, and the west filament is the B outflow (see previous section). While the knots of emission to the NW and SE fall on a line intersecting either star, inward extrapolation of the west filament and counter jet come closer to the infrared companion than the primary. Also, the midpoint of the C-D outflow falls close to the primary star, not the IRC (Böhm & Solf 1994). Other morphological evidence suggests that the primary star powers the NW-SE outflow and the infrared companion produces the east-west system. For example, the primary appears extended N-S in speckle interferometry measurements centered on the Hα line (Devaney *et al.* 1995). In addition, the H_2 $v=1-0S(1)$ emission from the companion is extended E-W and displaced somewhat to the west from the star in the direction of the west filament (Fig. 7).

On the other hand, the H_2 does not necessarily trace the flow itself. Instead, molecular hydrogen emission indicates the *interaction* of a wind with ambient material. A high velocity flow will produce shocks bright in H_2 only at the periphery, where the oblique impact angle permits efficient molecular line production (see previous section). Also, VLA radio continuum measurements of the T Tau system suggest that the IRC produces the more powerful wind (Schwartz *et al.* 1984), and the T Tau NW outflow is certainly more prominent than the east-west jet [Fig. 3 and Fig. 1 of van Langevelde *et al.* (1994)]. Finally, visible wavelength spectra of the T Tau primary show evidence for mass loss at velocities comparable to those seen to the west of T Tau (Mundt *et al.* 1984).

None of these arguments are conclusive, however, and the attribution of these outflows to their respective members of the T Tau binary must await imaging spectroscopy of high enough spatial resolution to cleanly separate the stars.

8. THE NATURE AND ORIGIN OF THE STELLAR LINE EMISSION

Figures 1, 2, and 7 demonstrate that molecular hydrogen line emission coincides with both components of the T Tau binary, with the infrared companion producing roughly one half of the total line strength. The Brγ transition, however, arises only in the primary. The following paragraphs discuss the nature and origin of these stellar spectral lines.

The T Tau primary seems an unlikely source of H_2 emission, since the strong Brγ line indicates a mechanism operating in the near vicinity of the star that is capable of ionizing hydrogen. If this mechanism is photoionization by ultraviolet radiation, the line ratios indicate that it is not likely to be the source of excitation of the infrared H_2 emission. We therefore conclude that the molecular hydrogen lines arise in gas heated to 2000–3000 K in shocks.

These shocks may occur as an outflow from the star interacts with the ambient molecular cloud. An intriguing possibility is that we are actually seeing the collimation of the outflows associated with T Tau NW and the west filament. As discussed in previous sections, the molecular hydrogen emission traces the edge of the flow. In this instance, the shocks would indicate a change in direction (i.e., collimation) rather than the oblique working surface of the jet. T Tau NW and the west filament are certainly collimated within 1″–2″ of the stars, and this picture naturally explains the morphological differences between the NW-SE outflow and the E-W system: the higher degree of collimation, slight curvature, and lack of gaps in the west filament indicate a channeling process taking place along the entire visible length of the flow. The NW-SE winds, on the other hand, do not become luminous between collimation near the star and the location where they strike the ambient molecular material.

Alternatively, the shocks may result from the impact of infalling gas on circumstellar matter, perhaps in the form of a disk. Herbst *et al.* (1995) propose such a scenario to explain the molecular hydrogen emission and large IR luminosity of the Haro 6–10 and UY Aur infrared companions. By assuming a spherical infall geometry, these authors derived an approximate relation between the observed $v=1-0S(1)$ line flux and the mass accretion rate, $\mathscr{M}$. The value of $\mathscr{M}$, along with an assumed ratio of column density to A_λ, gives the extinction to the photosphere, and $GM\mathscr{M}/r$ provides an estimate of the available accretion luminosity. The mass accretion rate in T Tau is approximately 10^{-7} $\mathscr{M}_\odot$ yr^{-1} for each star, using the stellar parameters derived in Koresko *et al.* 1996. This amount of infall can produce up to ~20 mag of visual extinction and ~3 $L_\odot$ of accretion luminosity. While this process can account for the unusual photometric properties of the infrared companion, it does not clarify why the primary star is not heavily extincted as well. A nonspherically symmetric geometry, such as infall onto a disk viewed nearly pole-on, would allow significant accretion luminosity, shock-heated H_2 emission, and relatively low A_V to the photosphere of the primary star.

An additional consequence of circumstellar matter deserves mention. Böhm & Solf (1994) did not see the counter jet to the east of T Tau, attributing the nondetection to a disk of projected radius ~2″ associated with the primary. They also invoked an obscuring disk of radius 0.″6 centered on the IRC to explain the apparent shift of the midpoint of the C-D outflow northward from the companion. Large, obscuring disks might explain these effects, as well as the gaps in the NW-SE outflow, but we would not favor this scenario without careful modeling. The stability of disks of size comparable to or larger than the binary separation is not guaranteed, particularly in the presence of significant and nonaligned outflows.

The recombination line emission is also interesting, since the *K* band spectral images presented here demonstrate that the primary star produces basically all the Brγ emission, (the T Tau binary emits Brackett lines in the *H* band as well, but poorer seeing on January 11 prevents identification with one or the other star). On the other hand, radio continuum measurements indicate that the ionized wind from the companion is ten times stronger than that from the primary (Schwartz *et al.* 1984). The reasons for this apparent discrepency are unclear, but the recent detection of circular polarization and

TABLE 2. H band diagnostics for shock heating vs ultraviolet fluorescence.

Line	Wavelength (μm)	Ratio to H_2 1-0 S(7) Line 2000K Shock[a]	UV Fluorescence[b]	Comment
4-2 O(3)	1.5095	5e-03	2.4	
5-3 O(2)	1.5603	2e-04	1.2	
6-4 Q(1)	1.6011	9e-05	1.9	telluric OII
7-5 Q(1)	1.7283	1e-05	1.4	telluric absorption
5-3 O(3)	1.6131	6e-04	2.1	telluric OH, H Br13
6-4 Q(3)	1.6158	1e-04	1.3	telluric OH, H Br13
5-3 O(5)	1.7355	5e-04	1.0	Br10

[a] from Smith, 1995. [b] from Black and van Dishoeck 1987.

rapid flux variations at $\lambda=18$ cm in T Tau suggest that a significant fraction of the IRC radio continuum emission is nonthermal (Phillips *et al.* 1993).

9. WHERE IS THE FLUORESCENT H_2?

Ultraviolet fluorescent excitation plays an important role in the UV H_2 emission lines observed with the *IUE* satellite (Brown *et al.* 1981, 1984). Presumably, this ultraviolet fluorescence will be accompanied by fluorescent emission in the infrared transitions, yet shock excitation seems to power all of the components of T Tau seen in the 2 μm molecular hydrogen lines. The two processes are not mutually exclusive. For example, the high temperatures we derive for the shock-heated gas ensure sufficient population of the $v,J=2,5$ lower state of the UV pumping transition leading to the ultraviolet H_2 lines (Brown *et al.* 1981, 1984; Black & van Dishoeck 1987).

Considerable discussion in recent years has centered on the best diagnostics to distinguish between shock heating and UV fluorescence as the excitation mechanism for H_2. Traditionally, astronomers have used the line strength ratio of the $v=1-0$ to the $v=2-1S(1)$ transition for this purpose, with ratios ~ 2 indicating fluorescence, and larger values pointing to shock heating (Black & Dalgarno 1976; Hollenbach & Shull 1977). In high density environments with intense ultraviolet radiation fields, however, collisional de-excitation of UV-pumped H_2 can heat the gas, leading to a level population for $v\leq 2$ approaching that of local thermodynamic equilibrium (LTE—Sternberg & Dalgarno 1989). Such conditions exist in H II regions, but are unlikely to appear near T Tau. Nevertheless, transitions with $v>2$ may be a more reliable indicator of ultraviolet fluorescence.

A number of these high v lines fall within the H photometric band and can serve as useful diagnostics. For example, Sternberg (1989) suggests using the $v=6-4Q$ branch near 1.6 μm The $v=1-0S(1)/v=6-4Q$ ratio is 3–6 for UV fluorescence and approximately 10^5 for gas in LTE at $T=2000$ K (Black & van Dishoeck 1987). Unfortunately, the brightest $v=6-4Q$ transition falls very close to strong, variable, terrestrial OH emission lines, reducing its usefulness at moderate spectral resolution. The best diagnostics will be those which avoid the OH, as well as strong hydrogen recombination lines, and regions of reduced atmospheric transparency.

Table 2 characterizes several H band diagnostic lines. The most promising H band discriminants are the $4-2O(3)$ and $5-3O(2)$ lines, whose respective ratios to the 1.75 μm $1-0S(7)$ transition are 2.4 and 1.2 for ultraviolet fluorescence, and 10^{-3} and 10^{-5} for shock heating (Black & van Dishoeck 1987; Smith 1995). We did not detect either of these higher-order transitions in the H band observations, while the $1-0S(7)$ is quite apparent in all regions of the frame, including the stars, T Tau NW, and the diffuse component. The formal upper limits to the line ratios indicate that UV fluorescence can account for at most 10%–15% of the near-infrared H_2 excitation. Thus, the 3D imaging spectra of T Tau do little to isolate the source of the UV fluorescence.

10. SUMMARY

We observed the near environment of T Tauri in the K and H photometric bands using the 3D spectral imager. As its name implies, this device produces three-dimensional data cubes, each slice of which covers 8×8 arcsec with 0.″5 pixels. The cubes span the entire photometric band at spectral resolution $\lambda/\Delta\lambda\sim 1000$. The CHARM tip-tilt module provided low-order wave-front correction.

Images centered at the wavelengths of quadrupole molecular hydrogen lines reveal extended emission centered on the stars, a filament extending to the west, diffuse radiation throughout the frame, and a knot of emission approximately 2 arcsec to the northwest. We detected this knot, called T Tau NW, in 11 H_2 transitions in the K and H band, as well as in two forbidden transitions of Fe II. The forbidden emission lies closer to the central stars than the molecular hydrogen. The Brγ line, on the other hand, is spatially unresolved and centered on the primary star. The strength ratio of H_2 lines sharing the same upper level can give an estimate of the extinction. We find that $A_V\sim 1.1$ toward T Tau NW, based on the $v=1-0$ $S(1)$ and $v=1-0$ $Q(3)$ lines.

Shock heating appears to be the major excitation mechanism in all five components revealed in molecular hydrogen: the primary star, the infrared companion, T Tau NW, the west filament, and the diffuse emission. When multiple lines are detected, a plot of the column density per degenerate sublevel versus energy level difference gives the excitation temperature under the assumption of local thermodynamic equilibrium. A range of excitation temperatures characterizes

the components of T Tau, from ~1000 K for the diffuse emission to ~3000 K near the stars. The derived temperatures allow an evaluation of the partition function and hence an estimate of the total column density and mass of molecular hydrogen in each component. In T Tau NW, the strengths of the even versus odd-J transitions are consistent with an ortho-to-para hydrogen ratio of 3.0, if each vibrational level experiences a single excitation temperature.

We believe that T Tau NW is a Herbig–Haro object, based on both spectroscopic and morphological evidence. This includes the presence of an apparent counter jet to the southeast and the displacement of the Fe II emission relative to the molecular hydrogen. The west filament also appears to be the signature of an outflow, and it, too, has a small counter jet to the east. We identify T Tau NW and its counterpart with the so-called C-D outflow found in visible wavelength, longslit spectra by Böhm & Solf (1994). The west filament and its counterpart are likely related to the B outflow, a conclusion supported by the apparent negative velocities and higher degree of collimation in this source. The near perpendicularity of T Tau NW and the west filament suggests that one star of the binary produces each outflow. Indirect evidence suggests that T Tau NW is associated with the primary, but definitive proof must await observations with higher spatial resolution.

Stellar H_2 line emission is very rare. In T Tau, we may be seeing oblique shocks resulting from the collimation of the T Tau NW and west filament outflows. Alternatively, accretion shocks can explain the large extinction and infrared luminosity of the T Tau infrared companion. Approximately 10^{-7} $M_\odot$ yr^{-1} of spherical infall can produce 3 $L_\odot$ of accretion luminosity and an $A_V \sim 20$. This process in its simplest form cannot account for the H_2 centered on the primary, however. Also unresolved is the apparent discrepancy between the infrared and radio wavelength tracers of ionized winds: the Brγ emission arises exclusively from the primary star, while the infrared companion dominates the radio continuum. Finally, we see no evidence for fluorescent molecular hydrogen emission in any of the components of the T Tau system.

The authors gratefully acknowledge the efforts of the entire FIASKO team in bringing the 3D instrument to the 3.5 m telescope. We also thank the CHARM team for adapting this device for use with 3D. T. H. thanks Chris Davis, Melvin Hoare, and Mike Smith for useful comments and suggestions.

REFERENCES

Adams, F. C. Lada, C. J., & Shu, F. H. 1988, ApJ, 326, 865
Beckwith, S., Gatley, I., Matthews, K., & Neugebauer, G. 1978, ApJ, 223, L41
Beckwith, S., Persson, S. E., & Neugebauer, G. 1979, ApJ, 227, 436
Bevington, P. R. 1969. Data Reduction and Error Analysis for the Physical Sciences (McGraw–Hill, New York)
Black, J. H., & van Dishoeck, E. F. 1987, ApJ, 322, 412
Black, J. H., & Dalgarno, A. 1976, ApJ, 203, 132
Böhm, K.-H., & Solf, J. 1994, ApJ, 430, 277
Bouchet, P., Manfroid, J., & Schmider, F. X. 1991, A&AS, 91, 409
Bragg, S. L., Brault, J. W., & Smith, W. H. 1982, ApJ, 263, 999
Brown, A., Jordan, C., Millar, T. J., Gondhalekar, P., & Wilson, R. 1981, Nature, 290, 34
Brown, A., Ferraz, M. C. de M., & Jordan, C. 1984, MNRAS, 207 831
Bührke, T., Brugel, E. W., & Mundt, R. 1986, A&A, 163, 83
Cohen, M., & Kuhi, L. V. 1979, ApJS, 41, 743
Devaney, M. N., Thiebaut E., Foy R., Blazit A., Bonneau D., Bouvier J., de Batz B., & Thom Ch. 1995, A&A, 300, 181
Dyck, H. M., Simon, T., & Zuckerman, B. 1982, ApJL, 255, L103
Ghez, A. M., Weinberger, A. J., Neugebauer, G., Matthews, K., & McCarthy, Jr., D. W. 1995, AJ, 110, 753
Ghez, A. M., Neugebauer, G., Gorham, P. W., Haniff, C. A., Kulkarni, S. R., Matthews, K., Koresko, C., & Beckwith, S. 1991, AJ, 102, 2066
Glindemann, A. H., *et al.* 1996 (in preparation)
Herbig, G. H. 1977, ApJ, 214, 747
Herbst, W., *et al.* 1986, ApJ, 310, L71
Herbst, T. M., Koresko, C. D., & Leinert, Ch. 1995, ApJL, 444, L93
Hollenbach, D. J., & Shull, J. M. 1977, ApJ, 216, 419
Koresko, C. D., Leinert, Ch., & Herbst, T. M. 1996 (in preparation)
Livingston, W., & Wallace, L. 1991, N. S. O. Technical Report 91-001 (digital version)
McQuarrie, D. A. 1976, Statistical Mechanics (Harper & Row, New York), p. 104
Mundt, R 1984, ApJ, 280, 749
Phillips, R. B., Lonsdale, C. J., & Feigelson, E. D. 1993, ApJ, 403, L43
Pradhan, A. K., & Zhang, H. L. 1993, ApJ, 409, L77
Rieke, G. H., & Lebofsky, M. J. 1985, ApJ, 288, 618
Schwartz, P. R., Simon, T., Zuckerman, B., & Howell, R. R. 1984, ApJ, 280, L23
Scoville, N. Z., Hall, D. N. B., Kleinmann, S. G., & Ridgway, S. T. 1982, ApJ, 253, 136
Shull, J. M., & Beckwith, S. 1982, ARA&A, 20, 163
Smith, M. D. 1991, MNRAS, 252, 378
Smith, M. D. 1995, A&A, 296, 789
Stapelfeldt, K. R., Beichmann, C. A. Hester, J. J., Scoville, N. Z., & Gautier III, T. N. 1991, ApJ, 371, 226
Sternberg, A. 1989, in Infrared Spectroscopy in Astronomy, ESA 5P290, p. 269
Sternberg, A., & Dalgarno, A. 1989, ApJ, 338, 197
Turner, J., Kirby-Docken, K., & Dalgarno, A. 1977, ApJS, 35 281
van Langevelde, H. J., van Dishoek, E. F., van der Werf, P. P., & Blake, G. A. 1994, A&A, 287, L25
Weitzel, L., Krabbe, A., Kroker, H., Thatte, N., Tacconi-Garman, L. E., Cameron, M., & Genzel, R. 1996, A&A, (submitted)

PLATE 141

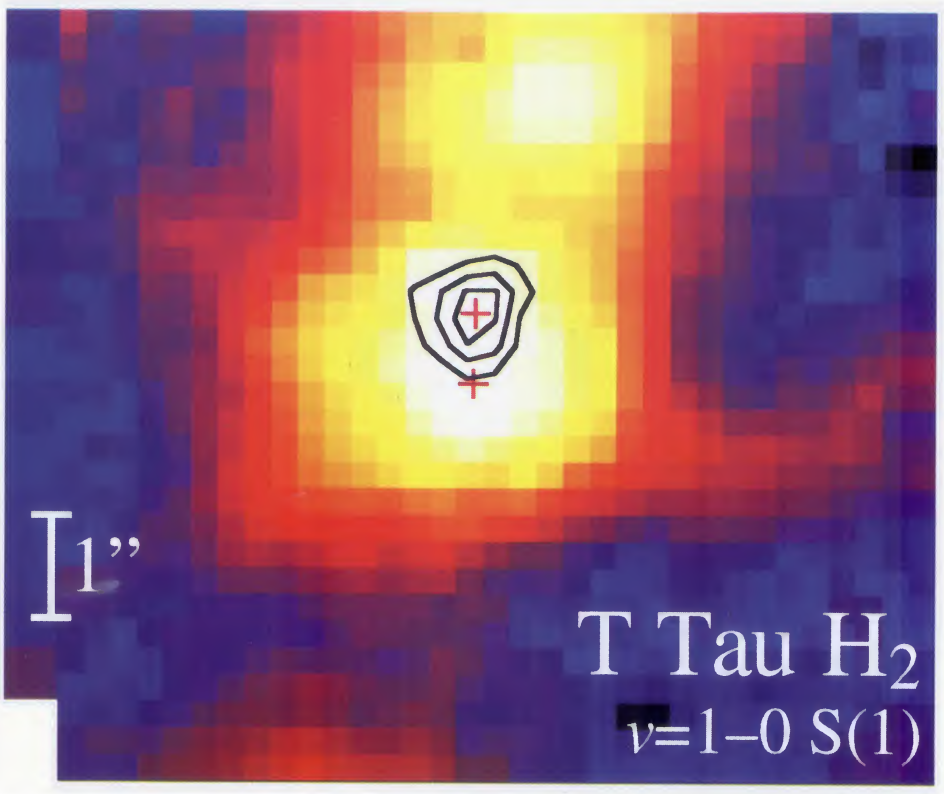

FIG. 2. A logarithmic stretch of the $S(1)$ image (colors), showing the location of the 2.12 μm continuum (contours), and the positions of the primary and IRC from Ghez *et al.* 1995 (upper and lower crosses, respectively). A counterpart to the northwest knot appears on the lower border of the frame, while a filament with smaller counterpart extends to the west.

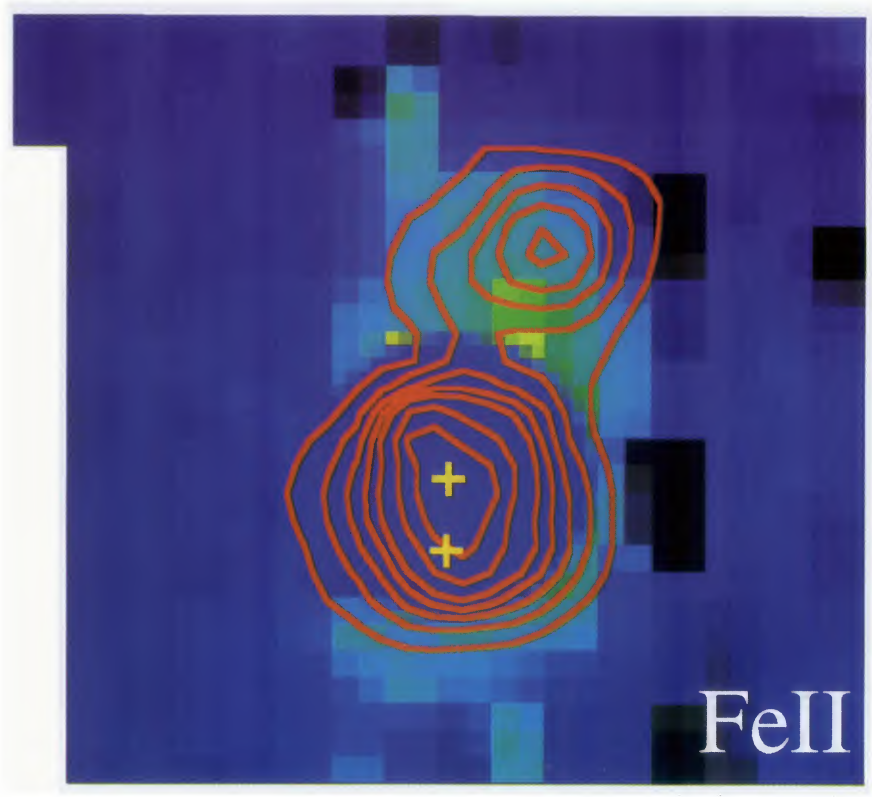

FIG. 3. Molecular hydrogen $v=1$–0 $S(1)$ emission (contours) superimposed on the Fe II image (colors). The crosses-again indicate the locations of the primary and infrared companion. The central 1.4 arcsec radius has been blanked out to eliminate noise associated with imperfect continuum subtraction on T Tau itself. This resulted from poorer seeing for the H band measurements. Note that the Fe II peaks closer to the binary than does the H_2.

Herbst *et al.* (see page 2404)

